Dalton Transactions

ROYAL SOCIETY OF CHEMISTRY

COMMUNICATION

View Article Online
View Journal | View Issue

Cite this: *Dalton Trans.*, 2024, **53**, 7677

Received 21st February 2024,
Accepted 8th April 2024

DOI: 10.1039/d4dt00509k

rsc.li/dalton

Simultaneous manipulation of iron(II) spin crossover and LIESST behaviour using pressure, temperature and light†

Gabriela Handzlik, *[a] Kamil F. Dziubek,[b] Michael Hanfland [c] and Dawid Pinkowicz *[a]

Spin crossover (SCO) and light-induced excited spin state trapping (LIESST) effects were studied using high pressure X-ray diffraction at cryogenic temperatures on a single crystal of the $\{[Fe^{II}(pyrazole)_4]_2[Nb^{IV}(CN)_8]\cdot 4H_2O\}_n$ (FeNb) coordination polymer. The studied compound does not show SCO or LIESST at ambient pressure, but these effects can be enforced by a mechanical stimulus. The obtained results demonstrate the manipulation of the spin state *via* the appropriate combination of multiple stimuli simultaneously.

Numerous spin crossover (SCO) materials have been extensively studied since the discovery of unusual thermal dependence of magnetisation of Fe^{III} compounds[1,2] and the first characterisation of the SCO of an Fe^{II}-based compound.[3] In its most common form, SCO is shown as a temperature-driven transition – the decrease in temperature leads to switching of $3d^4$–$3d^7$ metal ions from a high (HS) to low spin (LS) configuration. However, this type of spin state transition can also be induced by other factors, such as high pressure (HP) or absorption of photons. Triggering of the SCO behaviour using a variety of stimuli greatly expands the potential applications of these materials. The influence of pressure on the spin state was studied for the first time in the 1960s[4] while the light-induced spin state change was first reported in 1984.[5] The SCO transition driven by light is called light-induced excited spin state trapping (LIESST) and can occur in some SCO materials at low temperature, below the critical temperature called T_{LIESST}.[6–8] In most cases, evidence for the LIESST effect is shown as an increase in magnetisation due to the absorption of a visible light photon and it is rarely studied using single crystal X-ray diffraction (scXRD). This is because the observation of LIESST requires a very low temperature, usually well below the boiling point of liquid nitrogen which is not available in standard scXRD setups. The LIESST effect was characterised structurally for the first time in 2006 for compounds exhibiting LIESST at ambient pressure[9–12] but never under HP.

Switching the magnetic properties of materials by light is particularly interesting because photons enable remote control of the spin state and magnetisation. Other types of magnetic switching effects induced by light are associated with charge transfer (CT) in bimetallic compounds,[13–17] valence tautomerism (VT) in Co^{II}–dioxolene complexes[18–20] or ligand photoisomerization in lanthanide–diarylethene compounds[21–23] to name just a few. The photomagnetic effect based on CT was reported for Co^{II}–Fe^{III} [24] and Co^{II}–W^{V} [25] Prussian Blue (PB) analogues and exploited in core–shell PB nanoparticles.[26–28] The change in magnetisation in bimetallic compounds can also be caused by the light-induced spin state change at the single metal centre, such as the singlet–triplet excitation of Mo^{IV} or W^{IV}.[29–31] Recently, another mechanism of photomagnetic switching has been reported – spin state trapping by breaking the metal–cyanide bond,[32] which is conceptually similar to the light-driven coordination-induced spin state switching (LD-CISSS)[33,34] or ligand-driven light-induced valence tautomerism (LD-LIVT) in Co^{II}–dioxolene–styrylpyridine compounds.[35]

In this work we studied the high-pressure crystal structure of the cyano-bridged Fe^{II}–Nb^{IV} coordination polymer $\{[Fe^{II}(pyrazole)_4]_2[Nb^{IV}(CN)_8]\cdot 4H_2O\}_n$ **FeNb** at cryogenic temperatures with and without light irradiation (17 crystal structures). The presented results are the first demonstration of spin state manipulation *via* simultaneous control of three different parameters: temperature, pressure, and light.

The crystal structure and magnetic properties of **FeNb** under ambient pressure were previously reported by some

[a]*Faculty of Chemistry, Jagiellonian University, Gronostajowa 2, 30-387 Kraków, Poland. E-mail: gabriela.handzlik@uj.edu.pl, dawid.pinkowicz@uj.edu.pl*
[b]*Institut für Mineralogie und Kristallographie, Universität Wien, Josef-Holaubek-Platz 2, A-1090 Wien, Austria*
[c]*European Synchrotron Radiation Facility, 71 Avenue des Martyrs, CS40220, 38043 Grenoble, Cedex 9, France*

†Electronic supplementary information (ESI) available: Additional crystallographic tables and structural diagrams at various pressures and temperatures. CCDC 2326495, 2326497, 2326501, 2326507, 2326517, 2326519, 2326523, 2326553, 2326556, 2326557, 2326694, 2326697, 2327391, 2327431, 2327450, 2327700 and 2327702. For ESI and crystallographic data in CIF or other electronic format see DOI: https://doi.org/10.1039/d4dt00509k

of us.[36,37] Under these conditions, Fe^{II} ions are in the high spin (HS) state in the whole temperature range down to 1.8 K and the compound shows long-range magnetic ordering with T_c = 9.4 K. While no SCO effect was observed at ambient pressure, single crystal X-ray diffraction and Raman spectroscopy showed that a complete SCO transition can be induced by applying about 2.5–3.0 GPa at room temperature.

Magnetic measurements confirmed that at lower temperature the spin transition in **FeNb** occurs at lower applied pressure and the compound shows a pressure-induced LIESST effect at 2 K (at 0.6 GPa).[37]

FeNb crystallises in the tetragonal space group $I4_1/a$. Four of the eight cyanide ligands of the $[Nb(CN)_8]^{4-}$ anion coordinate to four Fe^{2+} cations, forming a 3-dimensional (3-D) diamond-like polymeric structure with niobium atoms as 4-fold nodes and iron atoms connecting these nodes (Fig. 1).

The remaining four cyanide ligands are terminal (non-bridging) and participate in hydrogen bonds with the crystallisation water molecules in the network. Each iron(II) centre is coordinated by six nitrogen atoms – two from the cyanide ligands in axial positions and four from monodentate pyrazole molecules in the equatorial plane (Fig. 1a). The pyrazole molecules are arranged in a helical fashion along the crystallographic *c* direction. Both left and right *pseudo*-helices are present.

In the previous study[37] the **FeNb** network was structurally characterised through a series of room temperature measurements under high pressure in the range of 0.0–2.9 GPa. The compression of the **FeNb** unit cell (Fig. 2, violet points) was found to be quite typical of molecular crystals. However, above 1.5 GPa the decrease of the unit cell volume was significantly faster suggesting pressure-induced SCO. On top of that, a contraction of the Fe–N bonds was observed above 1.5 GPa (Fig. 3) which is consistent with the SCO behaviour. Obviously, no LIESST was observed at room temperature.

This study provides insights into the pressure induced SCO and LIESST in **FeNb** at cryogenic temperatures and demonstrates that LIESST can only be observed in a specific pressure range. The irradiation of a single crystal under pressures below T_{LIESST} was experimentally challenging and impossible to realise with commercial setups. Therefore, it was performed at the HP beamline ID15B of the European Synchrotron Radiation Facility (ESRF).[38–40] The crystal structure of **FeNb** was determined under variable temperature and pressure conditions including light irradiation – seventeen datasets were collected for the same crystal, resulting in a set of seventeen crystal structures reported herein.

The first set of isothermal HP scXRD experiments was performed in the 0.08 to 1.53 GPa range at 100 K (pink points in Fig. 2, Fig. 3 and Table S1†). Up to 0.50 GPa the decrease of the unit cell volume is similar to that reported previously at room temperature (violet points in Fig. 2) and overall typical of molecular crystals. Above 0.80 GPa the unit cell volume starts to deviate significantly from the trend set in the 0.08–0.50 GPa range which strongly suggests pressure-induced SCO. The pressure dependence of the normalised unit cell volume (V/V_0 *vs.* p) of **FeNb** was fitted using the third-order Birch–Murnaghan

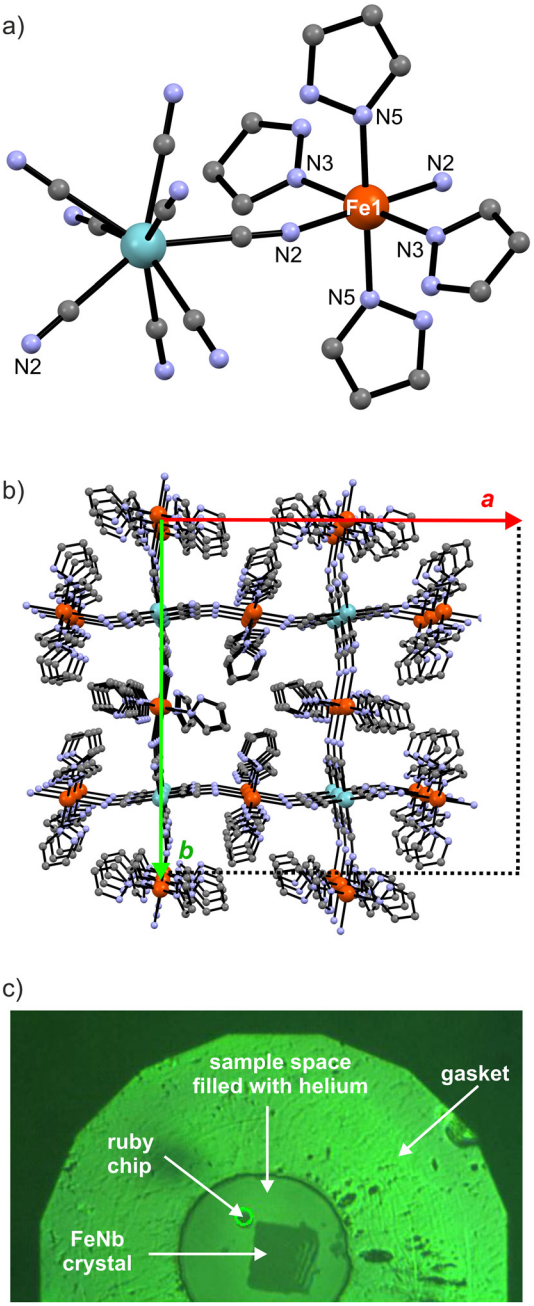

Fig. 1 Structural diagrams showing the molecular fragment of **FeNb** with the Fe^{II} coordination sphere labelling scheme (a) and the packing diagram along the *c* direction (b). H and O atoms are omitted for clarity. Fe – orange, Nb – cyan, C – grey, N – blue. Picture of the **FeNb** single crystal inside the membrane DAC (c).

equation of state (B–M EOS; eqn (1))[41,42] as previously done for room temperature pressure studies of a series of isostructural coordination polymers based on Mn^{II}, Fe^{II} and Ni^{II}:[43]

$$P(V) = \frac{3K_0}{2}\left[\left(\frac{V_0}{V}\right)^{\frac{7}{3}} - \left(\frac{V_0}{V}\right)^{\frac{5}{3}}\right]\left[1 + \frac{3}{4}(K'_0 - 4)\left(\left(\frac{V_0}{V}\right)^{\frac{2}{3}} - 1\right)\right] \quad (1)$$

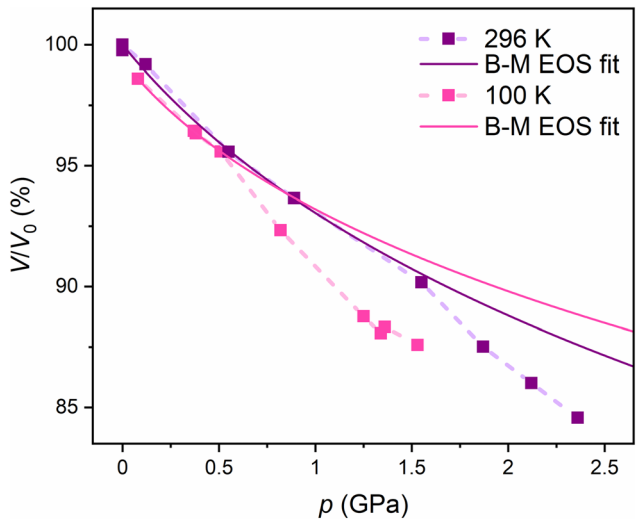

Fig. 2 Pressure dependence of the experimental **FeNb** unit cell volume at room temperature as reported in ref. 37 (violet points) and at 100 K (pink points; this work). Dotted lines are guides for the eye. The V_0 volume in the graph is the unit cell volume at room temperature and ambient pressure. Solid lines are the third-order Birch–Murnaghan EOS fits for both sets of experimental points in the 0.0–1.0 GPa range at RT and the 0.0–0.5 GPa range at 100 K.

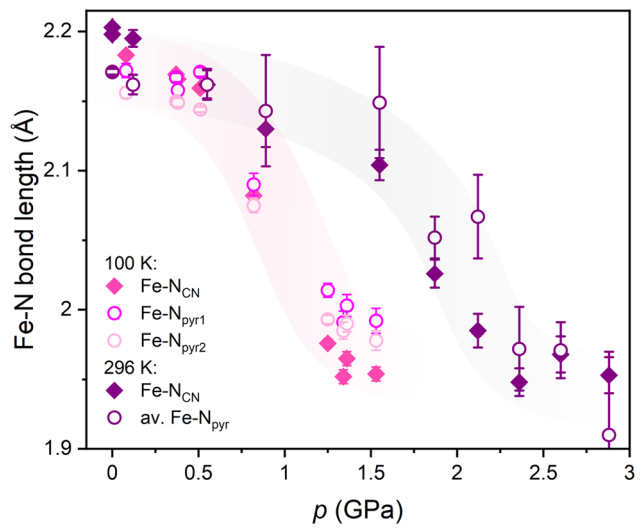

Fig. 3 Pressure dependence of the Fe–N bond lengths in **FeNb** with increasing pressure at 100 K (pink points) compared to the previous results at room temperature reported in ref. 37 (violet points). The accuracy of the bond length determination is visibly better from the data collected at lower temperature and using synchrotron radiation. The coloured ribbons behind the experimental points are only guides to the eye.

P – pressure, V – unit cell volume, V_0 – unit cell volume at ambient pressure, K_0 – isothermal bulk modulus at ambient pressure, K'_0 – dimensionless first derivative of K_0 with respect to pressure at a constant temperature.

At room temperature, the fit reproduces the experimental data very well in the range of 0.0–1.0 GPa (violet line in Fig. 2), yielding K_0 and K'_0 values of 10.1 ± 1.6 GPa and 9.0 ± 5.8 GPa, respectively. For measurements at 100 K, the fit reproduces the experimental points in a narrower range of 0.0–0.5 GPa, with K_0 and K'_0 values of 9.7 ± 1.1 GPa and 16.7 ± 6.0 GPa, respectively. Similar K_0 values at RT and 100 K indicate that the fitting ranges are correct.

The deviation of the experimental points from the B–M EOS marks the pressure value at which the pressure-induced SCO starts: 1.2 GPa at RT and 0.5 GPa at 100 K. As expected, the lower temperature allows the pressure-induced SCO to start at a lower pressure value. At a very low temperature (5 K), even lower pressure is required to induce the SCO transition in the **FeNb** network compared to that at 100 K.

The unit cell contraction under pressure observed above 1.5 GPa at RT and above 0.80 GPa at 100 K is caused by a significant change within the coordination sphere of Fe^{II} centres. At 100 K the average Fe–N bond lengths decrease from 2.17 Å at 0.1 GPa to 1.97 Å at 1.5 GPa (pink points in Fig. 3 and in Table S2†) while in the previous study at room temperature,[37] a much higher pressure *ca.* 2.3 GPa was required to achieve the same bond contraction (violet points in Fig. 3). The observed pressure-induced changes at 100 K are fully consistent with the SCO behaviour and with the pressure dependence of the Fe^{II}_{HS} fraction calculated from the magnetic data in ref. 37 (Fig. S5 in the ESI†).

Irradiation experiments were performed at the lowest achievable temperature T = 5 K using blue laser (488 nm, 150 mW) in nine experimental steps at three different pressures: 0.28(2) GPa (steps 1–3 in Fig. 4), 0.82(1) GPa (steps 4 and 5 in Fig. 4) and 0.87 (1) GPa (steps 6–9 in Fig. 4). According to the results of the magnetic measurements performed previously for **FeNb**, pressure values above 1.0 GPa completely hinder the LIESST effect, most probably due to the structural restraint of the Fe^{II} sites.[37]

At 0.28(2) GPa before irradiation the av. Fe–N bond length is 2.16(1) Å (typical of the HS configuration at low temperature) and is barely affected by blue light irradiation (steps 2 and 3) with Fe–N distances of 2.16(1) and 2.16(1) Å for the 1st and 2nd irradiation, respectively (Fig. 4 and Table S6†). Hence, the LIESST effect could not be observed because the pressure of 0.28(2) GPa does not induce the spin crossover transition – there are no LS Fe^{II} centers in the sample (steps 2 and 3). When the pressure is increased to 0.82(1) GPa, significant shortening of Fe–N bonds to 2.09(2) Å is observed in the dark (step 4 in Fig. 4 and Table S6†) compared to that at 0.28(2) GPa (step 1), indicating pressure-induced HS to LS transition. Irradiation at this pressure results in a small but non-negligible change in Fe–N bonds (step 5). Finally, increasing the pressure to 0.87(1) GPa (step 6) results in a further shortening of Fe–N bond lengths in the dark to av. 2.04(1) Å (Fig. 4, Fig. S1, S2 and Table S6†), consistent with the occurrence of nearly complete transition to the LS state (est. 80%). Blue light irradiation at 0.87(1) GPa (30 min of irradiation in step 7 and additional 30 min of irradiation in step 8) results in a pronounced increase of the Fe–N bond lengths to av. 2.09(1) Å, indicating the occurrence of the LIESST effect under pressure (Fig. 4 and Table S6†). After blue light irradiation at 0.87 GPa, the Fe–N_{CN} bonds are 2.6% longer and both Fe–N_{pyr} bonds are 2.0–2.1% longer than those before irradiation (step 6). Please

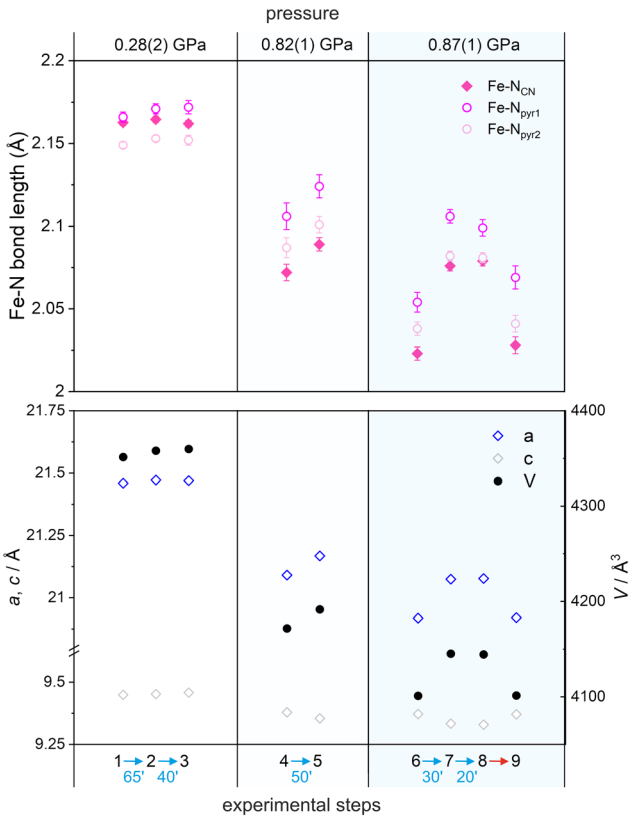

Fig. 4 The Fe–N bond lengths (top) and unit cell parameters (bottom) in nine consecutive HP experiments (1–9) at three different pressures and 5 K. Irradiation was done with 488 nm laser light (blue arrows). Thermal relaxation was carried out by heating the crystal to 60 K (red arrow) and cooling it back to 5 K while maintaining constant pressure. Error bars in the bottom plot are smaller than the size of the data points. Step 1 – before irradiation at 0.28(2) GPa, step 2 – after 1st 65 min of irradiation at 0.28(2) GPa, step 3 – after 2nd 40 min of irradiation at 0.28 (2) GPa, step 4 – before irradiation at 0.82(1) GPa, step 5 – after 50 min of irradiation at 0.82(1) GPa, step 6 – after relaxation at 60 K and before irradiation at 0.87(1) GPa, step 7 – after 1st 30 min of irradiation at 0.87(1) GPa, step 8 – after 2nd 30 min of irradiation at 0.87(1) GPa, step 9 – after thermal relaxation at 60 K and cooling back to 5 K.

note that the lack of differences in steps 7 and 8 is because the initial 30 min of irradiation is already enough to reach the maximum conversion to the photo-induced phase.

The photoexcited state can then be relaxed back to the initial state by heating the crystal to 60 K with Fe–N bonds going back to the av. 2.04(2) Å. The crystal structure after this thermal relaxation was again determined at 5 K and 0.87(1) GPa resulting in Fe–N bonds of *ca.* 2.04(2) Å (step 9; Fig. 4, Fig. S3, S4 and Table S6†). Similar trends were observed for the unit cell volume and unit cell parameters upon irradiation at different pressures (Fig. 4 bottom).

Conclusions

A series of seventeen high-pressure scXRD experiments carried out on the same single crystal of the $\{[Fe^{II}(pyrazole)_4]_2[Nb^{IV}(CN)_8]\cdot 4H_2O\}_n$ molecular magnet demonstrate simultaneous control of the spin state of Fe^{II} centres in this compound using pressure, temperature and light. It provides a basis for a better understanding of the complex magnetic behaviour of the studied compound at high pressure and low temperature. Previous structural studies of **FeNb** have only shown the effect of pressure at room temperature.[37] The results of the HP experiments presented here directly show the structural changes that occur in the **FeNb** structural framework at high pressure and low temperature. They also show how the structural changes induced by low temperature and pressure can be reversed in SCO compounds by light irradiation due to the pressure-induced LIESST effect, provided that the thermodynamic conditions are optimised. The presented results constitute the first example of high-pressure scXRD study with simultaneous SCO manipulation using temperature and light.

Crystallographic data for the structural analysis have been deposited with the Cambridge Crystallographic Data Centre. CCDC numbers: 2326694 (0.08 GPa, 100 K), 2326495 (0.37 GPa, 100 K), 2326697 (0.38 GPa, 100 K), 2326507 (0.51 GPa, 100 K), 2327450 (0.83 GPa, 100 K), 2326556 (1.25 GPa, 100 K), 2327431 (1.36 GPa, 100 K), 2327700 (1.53 GPa, 100 K), 2326497 (0.28 GPa, 5 K, before irradiation), 2326501 (0.28 GPa, 5 K, after 1st irradiation), 2326517 (0.28 GPa, 5 K, after 2nd irradiation), 2327702 (0.82 GPa, 5 K, before irradiation), 2326557 (0.82 GPa, 5 K, after irradiation), 2326519 (0.87 GPa, 5 K, before irradiation), 2326523 (0.87 GPa, 5 K, after 1st irradiation), 2326553 (0.87 GPa, 5 K, after 2nd irradiation), 2327391 (0.87 GPa, 5 K, after thermal relaxation). Source data are available through the ESRF DOI portal at **https://data.esrf.fr/doi/**.[44]

Conflicts of interest

There are no conflicts to declare.

Acknowledgements

This work was financed by the National Science Centre Poland within the Opus project 2020/37/B/ST5/02735. The authors would like to thank the European Synchrotron Radiation Facility for the beam time, experiment no. CH-6296 at the ID15B. Access to the ESRF was financed by the Polish Ministry of Education and Science – decision no. 2021/WK/11. The authors acknowledge Dr Michał Magott for insightful comments and vivid discussions.

References

1 L. Cambi and L. Szegö, *Ber. Dtsch. Chem. Ges.*, 1931, **64**, 2591–2598.
2 L. Cambi and L. Malatesta, *Ber. Dtsch. Chem. Ges.*, 1937, **70**, 2067–2078.

3 E. König and K. Madeja, *Chem. Commun. (London)*, 1966, 61–62.
4 A. H. Ewald, R. L. Martin, I. G. Ross and A. H. White, *Proc. R. Soc. London, Ser. A*, 1964, **280**, 235–257.
5 S. Decurtins, P. Gütlich, C. P. Köhler, H. Spiering and A. Hauser, *Chem. Phys. Lett.*, 1984, **105**, 1–4.
6 J.-F. Létard, *J. Mater. Chem.*, 2006, **16**, 2550–2559.
7 G. Chastanet, C. Desplanches, C. Baldé, P. Rosa, M. Marchivie and P. Guionneau, *Chem. Squared*, 2018, **2**, 2.
8 M. Nadeem, J. Cruddas, G. Ruzzi and B. J. Powell, *J. Am. Chem. Soc.*, 2022, **144**, 9138–9148.
9 C. Carbonera, J. Sánchez Costa, V. A. Money, J. Elhaïk, J. A. K. Howard, M. A. Halcrow and J.-F. Létard, *Dalton Trans.*, 2006, 3058–3066.
10 F.-F. Yan, W.-J. Jiang, N.-T. Yao, P.-D. Mao, L. Zhao, H.-Y. Sun, Y.-S. Meng and T. Liu, *Chem. Sci.*, 2023, **14**, 6936–6942.
11 R. Kulmaczewski, E. Trzop, L. J. Kershaw Cook, E. Collet, G. Chastanet and M. A. Halcrow, *Chem. Commun.*, 2017, **53**, 13268–13271.
12 A. L. Thompson, A. E. Goeta, J. A. Real, A. Galet and M. Carmen Muñoz, *Chem. Commun.*, 2004, 1390–1391.
13 T. Liu, H. Zheng, S. Kang, Y. Shiota, S. Hayami, M. Mito, O. Sato, K. Yoshizawa, S. Kanegawa and C. Duan, *Nat. Commun.*, 2013, **4**, 2826.
14 C. Mathonière, *Eur. J. Inorg. Chem.*, 2018, **2018**, 248–258.
15 R. Pełka, O. Stefańczyk, A. M. Majcher-Fitas, C. Mathonière and B. Sieklucka, *J. Magn. Magn. Mater.*, 2022, **544**, 168697.
16 E. S. Koumousi, I.-R. Jeon, Q. Gao, P. Dechambenoit, D. N. Woodruff, P. Merzeau, L. Buisson, X. Jia, D. Li, F. Volatron, C. Mathonière and R. Clérac, *J. Am. Chem. Soc.*, 2014, **136**, 15461–15464.
17 N.-T. Yao, L. Zhao, C. Yi, Q. Liu, Y.-M. Li, Y.-S. Meng, H. Oshio and T. Liu, *Angew. Chem., Int. Ed.*, 2022, **61**, e202115367.
18 O. Drath, R. W. Gable, B. Moubaraki, K. S. Murray, G. Poneti, L. Sorace and C. Boskovic, *Inorg. Chem.*, 2016, **55**, 4141–4151.
19 G. K. Gransbury, B. N. Livesay, J. T. Janetzki, M. A. Hay, R. W. Gable, M. P. Shores, A. Starikova and C. Boskovic, *J. Am. Chem. Soc.*, 2020, **142**, 10692–10704.
20 O. Sato, A. Cui, R. Matsuda, J. Tao and S. Hayami, *Acc. Chem. Res.*, 2007, **40**, 361–369.
21 N. El Beyrouti, F. Houard, M. Cordier, E. Trzop, S. Rigaut, B. Le Guennic, K. Bernot and L. Norel, *Chem. Commun.*, 2023, **59**, 5265–5268.
22 M. Hojorat, H. Al Sabea, L. Norel, K. Bernot, T. Roisnel, F. Gendron, B. L. Guennic, E. Trzop, E. Collet, J. R. Long and S. Rigaut, *J. Am. Chem. Soc.*, 2020, **142**, 931–936.
23 K. Rogacz, M. Brzozowska, S. Baś, K. Kurpiewska and D. Pinkowicz, *Inorg. Chem.*, 2022, **61**, 16295–16306.
24 O. Sato, T. Iyoda, A. Fujishima and K. Hashimoto, *Science*, 1996, **272**, 704–705.
25 S.-I. Ohkoshi, S. Ikeda, T. Hozumi, T. Kashiwagi and K. Hashimoto, *J. Am. Chem. Soc.*, 2006, **128**, 5320–5321.
26 M. F. Dumont, E. S. Knowles, A. Guiet, D. M. Pajerowski, A. Gomez, S. W. Kycia, M. W. Meisel and D. R. Talham, *Inorg. Chem.*, 2011, **50**, 4295–4300.
27 T. V. Brinzari, D. Rajan, C. F. Ferreira, S. A. Stoian, P. A. Quintero, M. W. Meisel and D. R. Talham, *J. Appl. Phys.*, 2018, **124**, 103904.
28 W. He, J. M. Cain, M. W. Meisel and D. R. Talham, *J. Mater. Chem. C*, 2021, **9**, 10830–10840.
29 S. Brossard, F. Volatron, L. Lisnard, M.-A. Arrio, L. Catala, C. Mathonière, T. Mallah, C. Cartier dit Moulin, A. Rogalev, F. Wilhelm, A. Smekhova and P. Sainctavit, *J. Am. Chem. Soc.*, 2012, **134**, 222–228.
30 N. Bridonneau, J. Long, J. L. Cantin, J. von Bardeleben, S. Pillet, E. E. Bendeif, D. Aravena, E. Ruiz and V. Marvaud, *Chem. Commun.*, 2015, **51**, 8229–8232.
31 M. Magott, O. Stefańczyk, B. Sieklucka and D. Pinkowicz, *Angew. Chem., Int. Ed.*, 2017, **56**, 13283–13287.
32 X. Qi, S. Pillet, C. de Graaf, M. Magott, E.-E. Bendeif, P. Guionneau, M. Rouzières, V. Marvaud, O. Stefańczyk, D. Pinkowicz and C. Mathonière, *Angew. Chem., Int. Ed.*, 2020, **59**, 3117–3121.
33 K. Fischer, J. Krahmer and F. Tuczek, *Z. Naturforsch., B*, 2022, **77**, 299–311.
34 S. Venkataramani, U. Jana, M. Dommaschk, F. D. Sönnichsen, F. Tuczek and R. Herges, *Science*, 2011, **331**, 445–448.
35 A. Witt, F. W. Heinemann and M. M. Khusniyarov, *Chem. Sci.*, 2015, **6**, 4599–4609.
36 D. Pinkowicz, R. Pełka, O. Drath, W. Nitek, M. Bałanda, A. M. Majcher, G. Poneti and B. Sieklucka, *Inorg. Chem.*, 2010, **49**, 7565–7576.
37 D. Pinkowicz, M. Rams, M. Mišek, K. V. Kamenev, H. Tomkowiak, A. Katrusiak and B. Sieklucka, *J. Am. Chem. Soc.*, 2015, **137**, 8795–8802.
38 D. Spahr, J. Binck, L. Bayarjargal, R. Luchitskaia, W. Morgenroth, D. Comboni, V. Milman and B. Winkler, *Inorg. Chem.*, 2021, **60**, 5419–5422.
39 D. Paliwoda, D. Comboni, T. Poręba, M. Hanfland, F. Alabarse, D. Maurin, T. Michel, U. B. Demirci, J. Rouquette, F. di Renzo, A. van der Lee, S. Bernard and J. Haines, *J. Phys. Chem. Lett.*, 2021, **12**, 5059–5063.
40 T. Poręba, D. Comboni, M. Mezouar, G. Garbarino and M. Hanfland, *J. Phys.: Condens. Matter*, 2023, **35**, 054001.
41 F. Birch, *Phys. Rev.*, 1947, **71**, 809–824.
42 F. Birch, *J. Geophys. Res.: Solid Earth*, 1978, **83**, 1257–1268.
43 D. Pinkowicz, A. Katrusiak and H. Tomkowiak, in *Comprehensive Coordination Chemistry III*, ed. E. C. Constable, G. Parkin and L. Que Jr., Elsevier, Oxford, 2021, pp. 546–556.
44 D. Pinkowicz, G. Handzlik, K. Dziubek and M. Magott, *Pressure induced spin crossover photomagnet: crystal structure determination below the magnetic ordering temperature of 10 K under high pres [dataset]*, European Synchrotron Radiation Facility, 2025, DOI: 10.15151/ESRF-ES-708312219.